Title

MATHEMATICAL MODELING OF LIQUID-JUNCTION PHOTOVOLTAIC CELLS: II. EFFECT OF SYSTEM PARAMETERS ON CURRENT-POTENTIAL CURVES

Authors

Orazem, M.E.
Newman, J.

Publication Date

1983-06-01

Lawrence Berkeley Laboratory
UNIVERSITY OF CALIFORNIA

Materials & Molecular Research Division

Submitted to the Journal of the Electrochemical Society

MATHEMATICAL MODELING OF LIQUID-JUNCTION PHOTOVOLTAIC CELLS: II. EFFECT OF SYSTEM PARAMETERS ON CURRENT-POTENTIAL CURVES

M.E. Orazem and J. Newman

June 1983

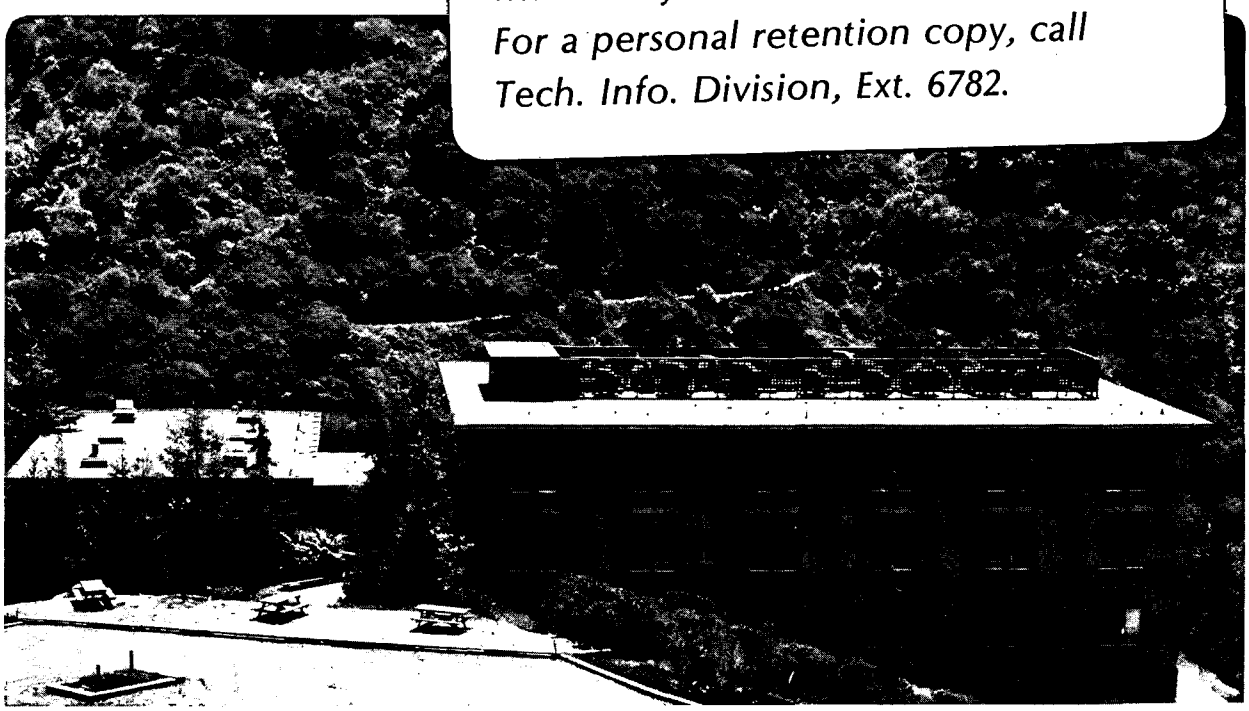

Prepared for the U.S. Department of Energy under Contract DE-AC03-76SF00098

DISCLAIMER

LBL-16211

Mathematical Modeling of Liquid-Junction Photovoltaic Cells:

II. Effect of System Parameters on Current-Potential Curves

Mark E. Orazem and John Newman

Materials and Molecular Research Division, Lawrence Berkeley Laboratory, and Department of Chemical Engineering, University of California, Berkeley, California 94720

June 1983

ABSTRACT

The one-dimensional mathematical model presented in a previous paper was used to calculate the effect of system variables on the performance of an n-type GaAs semiconducting anode in contact with an 0.8 M K_2Se, 0.1 M K_2Se_2, 1.0 M KOH electrolytic solution. The performance of the semiconductor electrode is influenced by kinetic limitations to interfacial reactions, dopant concentration, semiconductor thickness, the direction of illumination, and the amount of light absorbed in the semiconductor. An optimal dopant concentration and semiconductor thickness can be calculated for a given system.

Key words: Semiconductor, Electrode, Solar, Energy Conversion.

The liquid-junction photovoltaic cell is an electrochemical system with one or two semiconducting electrodes. This system has undergone intense study since the early 1970's as a means of converting solar energy to chemical or electrical energy.[1-8] A number of articles review the physics of the liquid-junction cell, the role of the semiconducting electrode, and the literature (see, e.g., references 9-19).

A mathematical model of the liquid-junction photovoltaic cell was presented in a previous paper.[20] The results of the model, obtained through numerical computation, are used here to gain insight into the cell behavior and into the factors influencing cell design. This model can also be coupled with primary resistance calculations to optimize the design of cell configurations.[21]

1. INTRODUCTION

A one-dimensional mathematical model of the liquid-junction photovoltaic cell has been developed[20] which treats explicitly the semiconductor, the electrolyte, and the semiconductor-electrolyte interface in terms of potentials and concentrations of charged species. A one-dimensional representation of the model is presented in Figure 1. This model includes macroscopic representations of the counterelectrode, the electrolytic solution, and the semiconductor coupled with a microscopic representation of the interface between the semiconductor and the solution. The semiconductor-electrolyte interface couples the macroscopic equations which govern the adjacent bulk phases.

The interface is represented by four planes, inner and outer Helmholtz planes on the electrolyte side of the interface and inner and outer surface states on the semiconductor side. The outer Helmholtz plane (OHP) is the

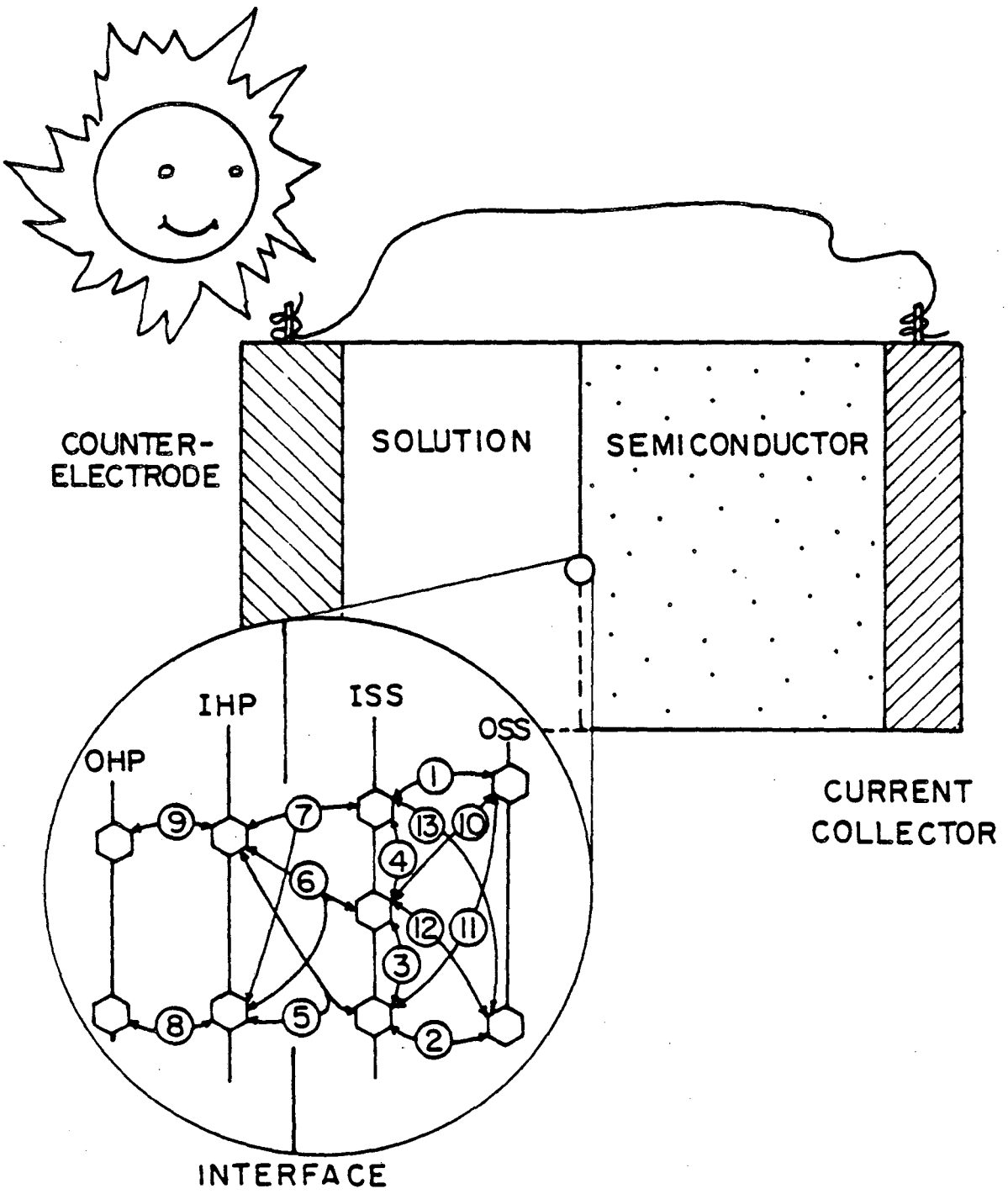

XBL 835-9621

Figure 1. Mathematical model of the liquid-junction photovoltaic cell.

plane of closest approach for (hydrated) ions associated with the bulk solution. The inner Helmholtz plane (IHP) passes through the center of ions specifically adsorbed on the semiconductor surface. The outer surface state (OSS) represents the plane of closest approach for electrons (and holes) associated with the bulk of the semiconductor. The inner surface state (ISS) is a plane of surface sites for adsorbed electrons.

This model of the semiconductor-electrolyte interface is an extension of the classical diffuse double-layer theory.[22-24] Charge adsorbed onto the IHP and the ISS planes is balanced by charge in the diffuse region of the electrolyte and the space-charge region of the semiconductor. The net charge of the interface, including surface planes and diffuse and space-charge regions, is equal to zero.

Within the model, single-step reactions relate concentrations and potentials at interfacial planes. A continuous spectrum of energy levels at the ISS is represented by three discrete energy levels (designated v, t, and c). Conduction electrons are adsorbed via reaction 1 (see INTERFACE in Figure 1) from the OSS to high-energy sites at the ISS, via reaction 10 to intermediate-energy sites at the ISS, and via reaction 11 to low-energy sites at the ISS. Via reaction 2, low-energy electrons at the ISS can occupy vacancies in the valence band, or holes, at the OSS. Intermediate-energy electrons can transfer from the ISS to the OSS through reaction 12 and high-energy electrons can transfer through reaction 13. Reactions 3 and 4 allow the shifting of electrons from one energy level to another.

Ionic species from the solution are adsorbed onto the IHP by reactions 8 and 9. Two adsorbed species are considered here. It is assumed that other ionic species in the solution do not adsorb and do not participate in

the electrochemical reactions. Relaxation of this assumption involves the inclusion of additional ion-adsorption and charge-transfer reactions. Reactions 5, 6, and 7 are the charge-transfer reactions that take place among adsorbed ions at the IHP and adsorbed high, intermediate, or low-energy electrons at the ISS. Charge-transfer reactions allow passage of electrical current from the semiconductor to the solution.

The coupled nonlinear ordinary differential equations of the model were posed in finite-difference form and solved numerically. The coupled, nonlinear equations presented for the liquid-junction cell were solved numerically for the cell under equilibrium and steady-state conditions.[25] The equations were properly linearized, posed in finite-difference form, and solved using Newman's BAND method,[26] coupled with Newton-Raphson iteration. Calculation of a current-potential curve involved iterative solution of the system of coupled equations for input values of solar illumination and current density.

2. RESULTS

Computed results for the mathematical model of the liquid-junction photovoltaic cell are presented in the following section. The parameter values chosen for the model are consistent with an n-type GaAs anode in contact with an 0.8 M K_2Se, 0.1 M K_2Se_2, 1.0 M KOH solution. The redox couple was assumed to be Se_2^{2-}/Se^{2-}, and the semiconductor was illuminated at the semiconductor-electrolyte interface. Input parameter values are as presented in Tables 1 through 3 unless stated otherwise. Dependent parameters calculated from the input data are presented in Table 4.

The n-type GaAs system was chosen for analysis to allow comparison to the experimental work of Heller and Miller.[8,27,28] Their cell achieved a 12

Table 1. Input Parameters for the Semiconductor

Semiconductor: n-GaAs		
Valence band site concentration	N_v	1.16×10^{-5} mol/cm^3
Conduction band site concentration	N_c	7.80×10^{-7} mol/cm^3
Band gap	E_g	1.4 eV
Dopant concentration	$N_d - N_a$	9.96×10^{-8} equiv/cm^3
Electron diffusivity	D_{e^-}	222.0 cm^2/s
Hole diffusivity	D_{h^+}	6.46 cm^2/s
Permittivity	ε_{sc}	1.06×10^{-12} C/V-s
Solar absorption coefficient	m	4.40×10^{-5} cm^{-1}
Solar spectrum efficiency	η	0.3735
Total incident radiation (AM-2)	q_o	7.139×10^{-7} mol/cm^2-s 882 W/m^2
Homogeneous recombination rate constants:	$N_t k_2$	1.89×10^9 s^{-1}
	$(k_1 N_v + k_3 N_c)/k_4$	100.
	k_2/k_4	2.56×10^{-3} cm^3/mol

Table 2. Input Parameters for the Semiconductor-Electrolyte Interface

ISS site	k	v	t	c	
ISS site energy	E_k	1.3	1.4	1.5	eV
ISS site density	γ_k	0.3334	0.3333	0.3333	

Total ISS site concentration	Γ_{iss}	4.019×10^{-12} mol/cm^2
Total IHP site concentration	Γ_{ihp}	1.200×10^{-13} mol/cm^2
IHP adsorption energy	ΔE_3	0.0 J/mol
	ΔE_4	0.0 J/mol
Equilibrium OSS potential	Φ_{oss}	5.93 mV
Equilibrium charge on interface		-0.1298 μC/cm^2
Distance between OSS and ISS	δ_1	1.0×10^{-8} cm
Distance between ISS and IHP	δ_2	2.0×10^{-8} cm
Distance between IHP and OHP	δ_3	2.0×10^{-8} cm
Permittivity between ISS and IHP	ε_2	6.93×10^{-12} C/V-cm
Rate constants:		
(OSS-ISS)	k_{etr}	1.0×10^{25} cm^3/mol-s
(ISS)	k_{sft}	1.0×10^{29} cm^2/mol-s
(ISS-IHP)	k_{cht}	1.0×10^{29} cm^2/mol-s
(IHP-OHP)	k_{ads}	1.0×10^{23} s^{-1}

Table 3. Input Parameters for the Electrolyte

Electrolyte: 0.8 M K_2Se, 0.1 M K_2Se_2, 1.0 M KOH						
Species index	k	1	2	3	4	
Species		K^+	OH^-	Se_2^{2-}	Se^{2-}	
Charge number	z_k	+1	-1	-2	-2	
Bulk concentration	$c_{k,\infty}$	0.0028	0.0010	0.0001	0.0008	mol/cm^3
Diffusivity (x10^5)	D_k	1.957	5.260	1.000	1.000	cm^2/s
Permittivity		ε_{sol}			6.930x10^{-12}	C/V-cm
Conductivity		κ			0.3	$(\Omega\text{-cm})^{-1}$
Temperature		T			300.	K

Table 4. Values Calculated from Input Parameters

Semiconductor:		
Fermi level	E_f	1.347 eV
Intrinsic concentration	n_i	5.228×10^{-18} mol/cm^3
Minority carrier diffusion length	L_p	5.846×10^{-4} cm
Debye length	λ_{sc}	1.689×10^{-6} cm
Electrolyte:		
Debye Length	λ_{sol}	1.967×10^{-8} cm

percent power efficiency based upon incident radiation, an open circuit potential of 0.7 volts, and a closed circuit current of 24 mA/cm^2. A description of their experimental electrodes, cell, and measuring techniques is presented in reference (29). Their cell efficiency includes the effects of reflection losses and electrolyte resistance. The influence of kinetic and mass-transfer limitations to current flow at the countrelectrode were reduced by using a counterelectrode to semiconductor area ratio of 50. The Se_2^{2-}/Se^{2-} redox couple was chosen to limit the corrosion of GaAs under 1000 W/m^2 illumination to a few micrometers per year (approximately 0.04 mA/cm^2).[30-32]

The discussion of the effect of kinetic, bulk semiconductor, and interfacial parameters does not include the effect of IR drop in the electrolyte or kinetic and mass-transfer limitations at the counterelectrode (see section 3.5 of reference 20). The contribution of these phenomena is

discussed in section 2.3.1 (see also reference 21).

2.1. Interfacial Kinetic Limitations

The values of the interfacial rate constants can affect the open-circuit cell potential, the value of the limiting current, and the shape of the current-potential curve. Most (>99 percent) of the recombination under open-circuit illumination occurs at the interface. Homogeneous recombination is included in the model but does not play a major role for the range of parameters studied.

2.1.1. Ion-adsorption reactions. Current-potential curves are presented in Figure 2 with the interfacial rate constant for adsorption and desorption of ions onto the inner Helmholtz plane as a parameter (reactions 8 and 9 in Figure 1). In each case the cell potential is a maximum at open circuit (700.5 mV) and decreases as the anodic current increases. A limiting current is observed due to limitations of mass transfer and generation of holes in the semiconductor.

The ion-adsorption rate constant influences the limiting current and the shape of the current-potential curve. A dramatic decrease in the maximum power obtained from this system is observed for the cases with small ion-adsorption rate constants. Kinetic limitations to ion adsorption are seen to have a major effect on cell performance.

Concentration distributions of holes and electrons in the semiconductor are presented in Figures 3 and 4 for a system with no interfacial kinetic limitations and for a system with kinetic limitations to ion adsorption, respectively. The equilibrium and illuminated open-circuit concentration distributions for the two cases are identical. Under

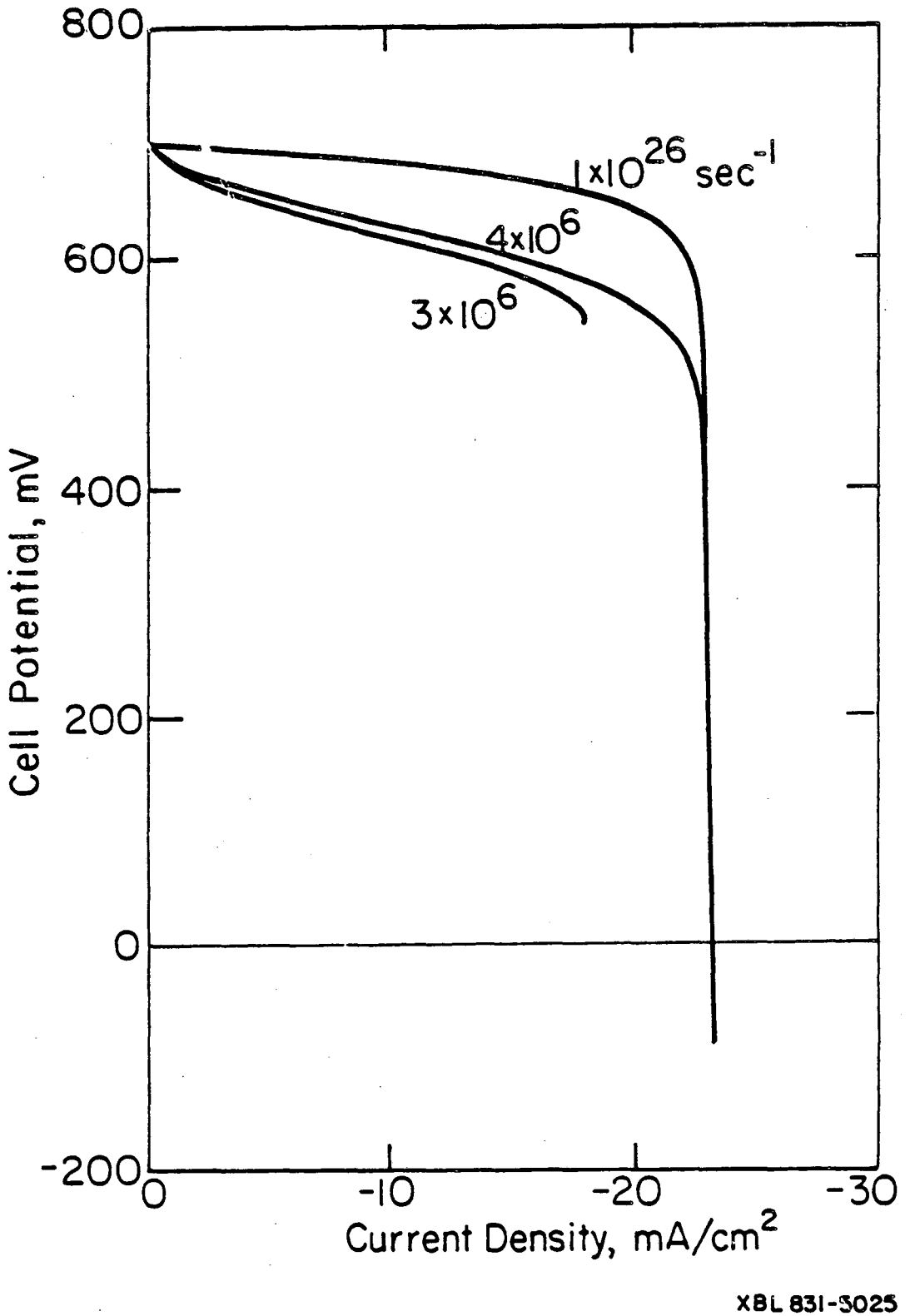

Figure 2. Computer current-potential curves for an n-type GaAs Anode with ion-adsorption rate constant as a parameter.

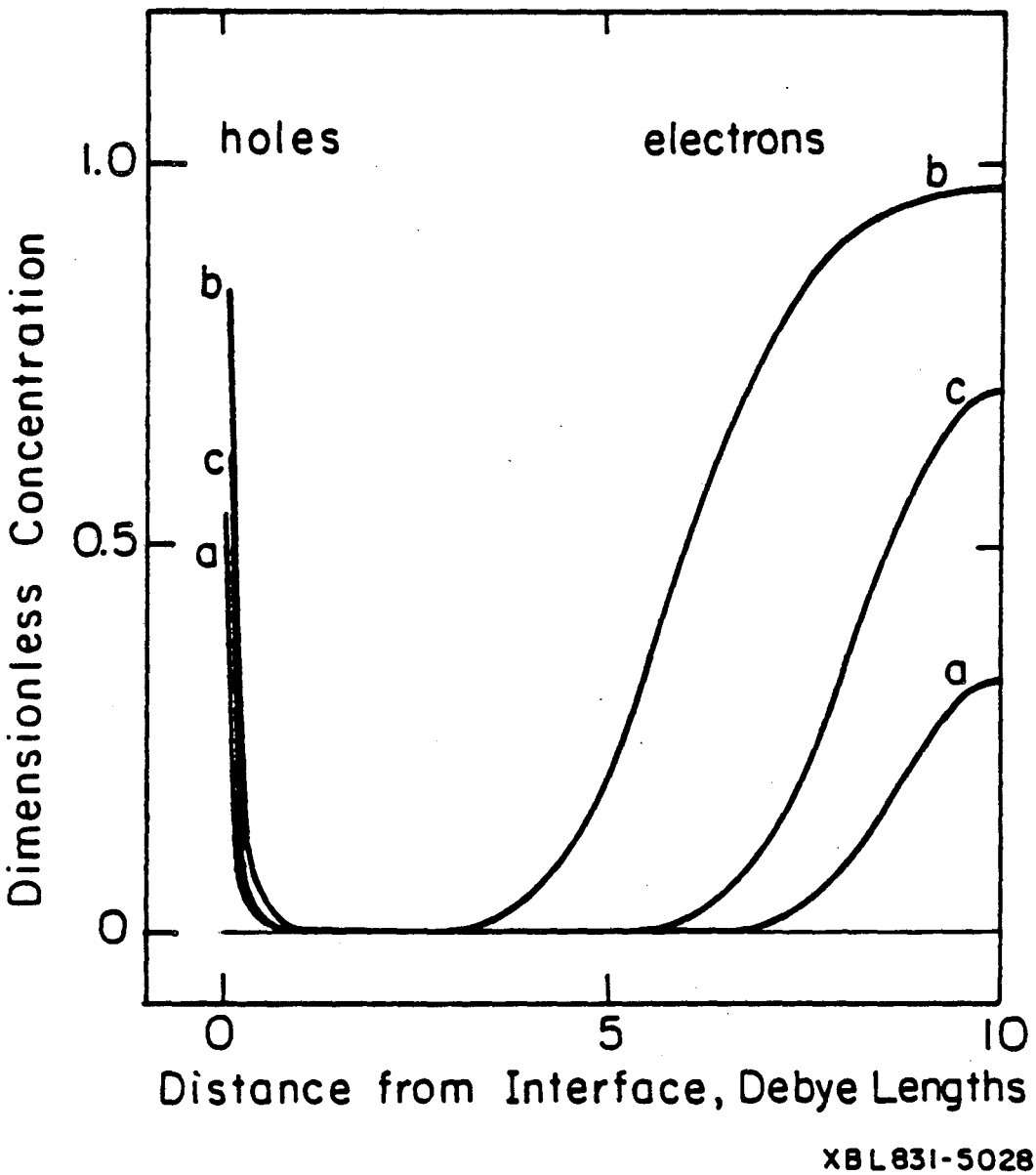

Figure 3. Concentration distribution for the liquid-junction cell with no kinetic limitations (k_{ads} = 1.0x10^{26} s^{-1}). Curve a, open circuit in the dark; curve b, open circuit under illumination; and curve c, near short circuit (i = -23.1 mA/cm^2) under illumination.

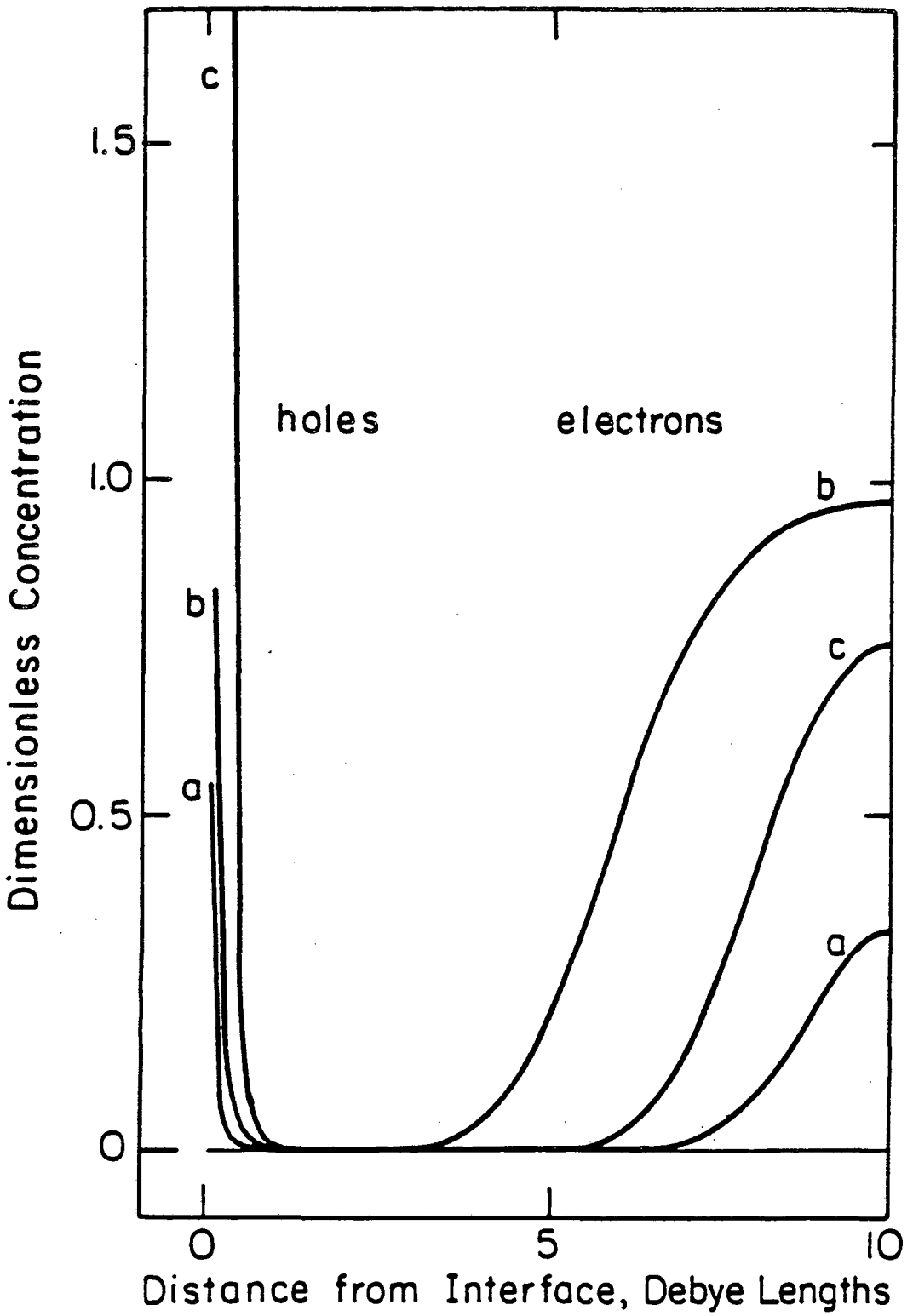

Figure 4. Concentration distribution for the liquid-junction cell with kinetic limitations to ion adsorption ($k_{ads} = 4.x10^6\ s^{-1}$). Curve a, open circuit in the dark; curve b, open circuit under illumination; and curve c, near short circuit ($i = -23.1\ mA/cm^2$) under illumination.

equilibrium conditions the concentration of holes (curve a) is essentially zero in the bulk of the semiconductor and increases near the negatively charged interface. Conduction electrons are depleted near the interface and reach a value of 0.328 dimensionless units at the current collector, where the concentrations are scaled by the dopant concentration ($N_d - N_a$). The electron concentration in a neutral region of the semiconductor would have a value essentially equal to 1.0. The equilibrated semiconductor of Figure 3 can therefore be described as having an inversion region extending from the semiconductor-electrolyte interface to 0.5 Debye lengths from the interface and a depletion region extending to the current collector.

The positive background charge density has a value of 1.0; the semiconductor has a net positive charge which is balanced by charge associated with the diffuse region of the electrolyte and the interface. System electroneutrality is maintained. The potential gradient, the driving force for migration of charged species, is balanced by the concentration gradient, which drives diffusion. The net flux of each species in the semiconductor is equal to zero at equilibrium.

Illumination under open-circuit conditions produces electron-hole pairs, which are separated by the potential gradient. The concentration of holes increases near the interface, and the concentration of electrons increases near the current collector (curve b). As the system without kinetic limitations approaches short circuit (curve c in Figure 3), the concentrations of holes and electrons approach the equilibrium distributions. The system under kinetic limitations to ion adsorption, in contrast, experiences an increase in hole concentration at large current densities (curve c in Figure 4).

The model also allows calculation of the potential distribution in the semiconductor and throughout the cell. Kinetic limitations at the interface are compensated by increased changes of potential across the reaction planes. A small ion-adsorption rate constant is therefore compensated by increased potential and concentration driving forces at the interface. In this way, kinetic limitations influence the cell performance.

2.1.2. Charge-transfer reactions. Current-potential curves are presented in Figure 5 with the rate constant for charge transfer from the inner surface states of the semiconductor to the inner Helmholtz plane as a parameter (reactions 5, 6, and 7 in Figure 1). The cell potential has a maximum value under open-circuit illumination and decreases as the anodic current increases. Kinetic limitations to charge transfer adversely influence the power performance of the cell. A small charge-transfer rate constant is compensated by increased potential and concentration driving forces.

2.1.3. Electron-adsorption reactions. The influence of electron-adsorption rate constants (reactions 1, 2, 10, 11, 12, and 13 in Figure 1) upon the current-potential curve is presented in Figure 6. A small electron-adsorption rate constant reduces the net rate of recombination of holes and electrons at the surface and thus increases both the cell potential and the value of the limiting current.

2.1.4. Surface-shift reactions. The rate constants for reactions which allow electrons to move from one energy level at the interface to another (reactions 3 and 4 in Figure 1) do not have any independent effect upon the cell potential or the value of the limiting current. These rate constants

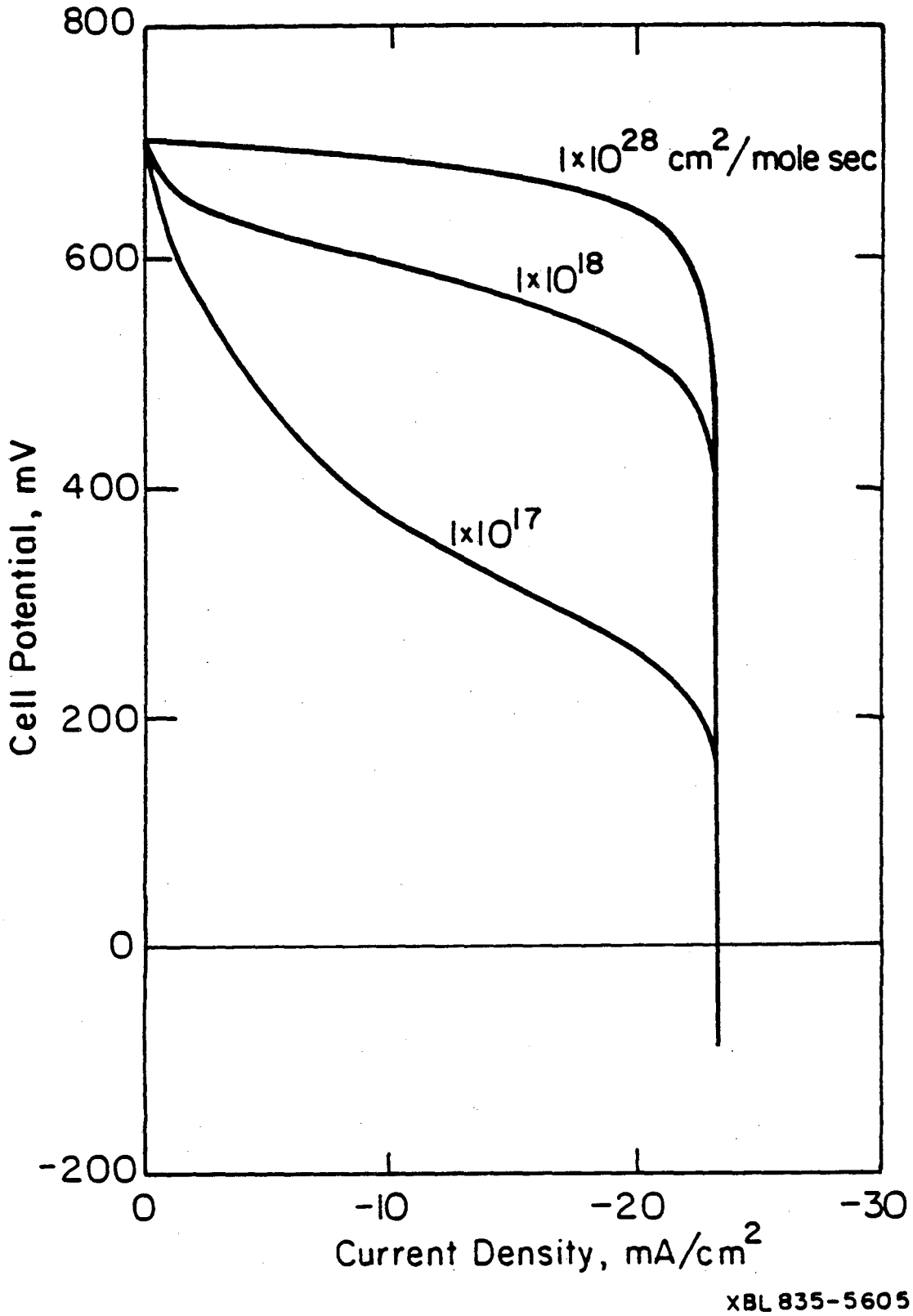

Figure 5. Computer current-potential curves for an n-type GaAs Anode with charge-transfer rate constant as a parameter.

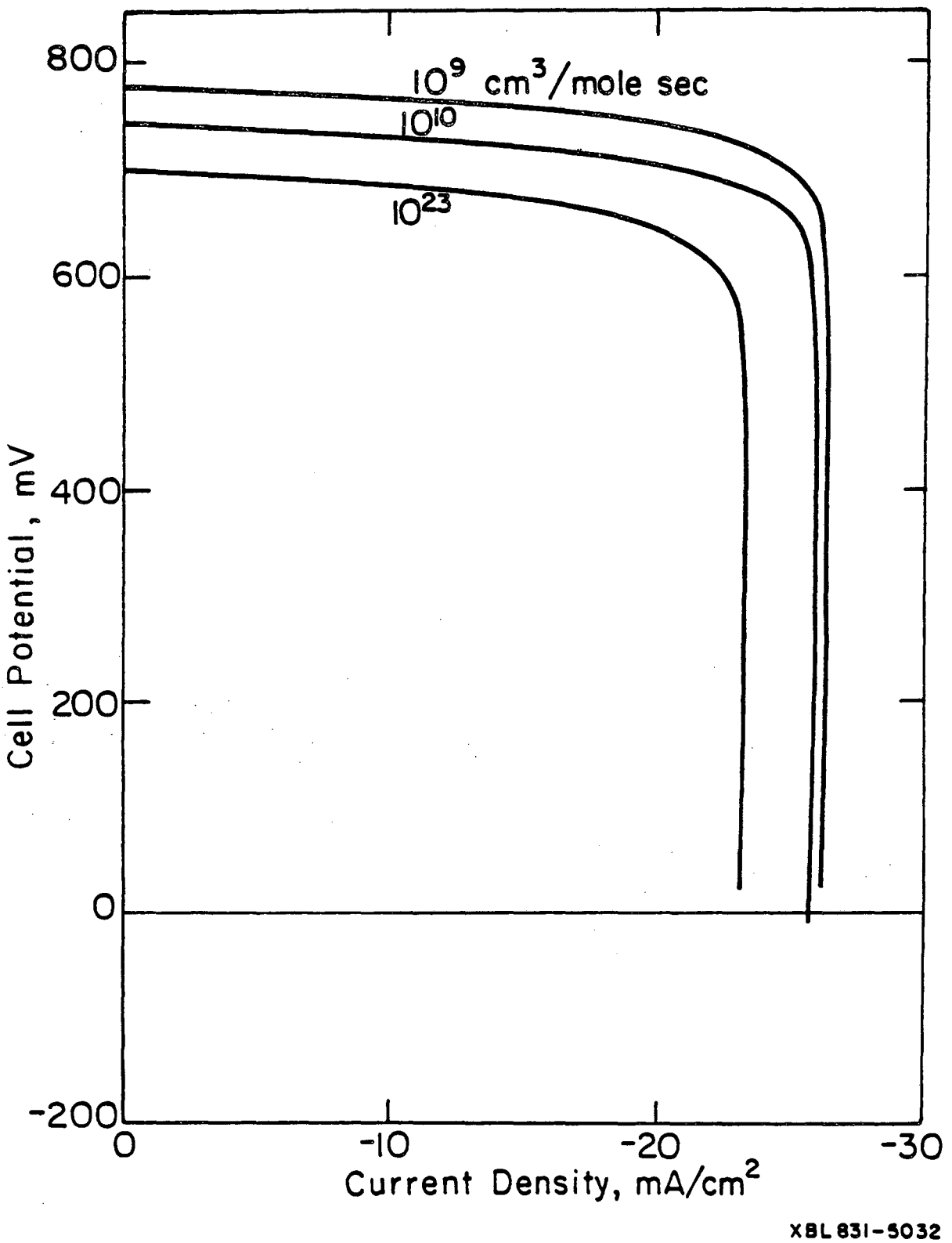

Figure 6. Computer current-potential curves for an n-type GaAs anode with electron-adsorption rate constant as a parameter.

affect only the path by which recombination may take place.

2.2. Bulk Semiconductor Properties

Bulk semiconductor properties can greatly influence the performance of the liquid-junction photovoltaic cell. Some properties which can be controlled in semiconductor manufacture and cell design are the dopant concentration, the thickness of the semiconductor, the solar absorption coefficient, and the amount of light absorbed in the semiconductor.

2.2.1. Dopant concentration. Current-potential curves are presented in Figure 7 for concentrations of positive background charge ranging from 2.500×10^{-7} to 0.0396×10^{-7} equivalents/cm^3 and for a semiconductor thickness of 10 Debye lengths. The cell performance is strongly dependent upon doping level. The influence of illumination on the potential variation in the semiconductor is greatest with a small dopant concentration; thus in this case a large open-circuit cell potential is observed. The low concentration of charge-carrying species in the neutral region is associated with a large resistance to current flow in the semiconductor and with enhanced homogeneous recombination of electron-hole pairs; thus a small limiting current is observed. Conversely, a large dopant concentration is characterized by a small open-circuit potential and a large limiting current.

The semiconductor Debye length is inversely proportional to the square root of the dopant concentration. If the semiconductor thickness were held constant at a value of 1.69×10^{-5} cm, as opposed to 10 Debye lengths, similar results would be observed for high dopant concentrations. At low dopant concentrations, the semiconductor thickness would be smaller than the space-charge region thickness, and the cell potential would be reduced (see

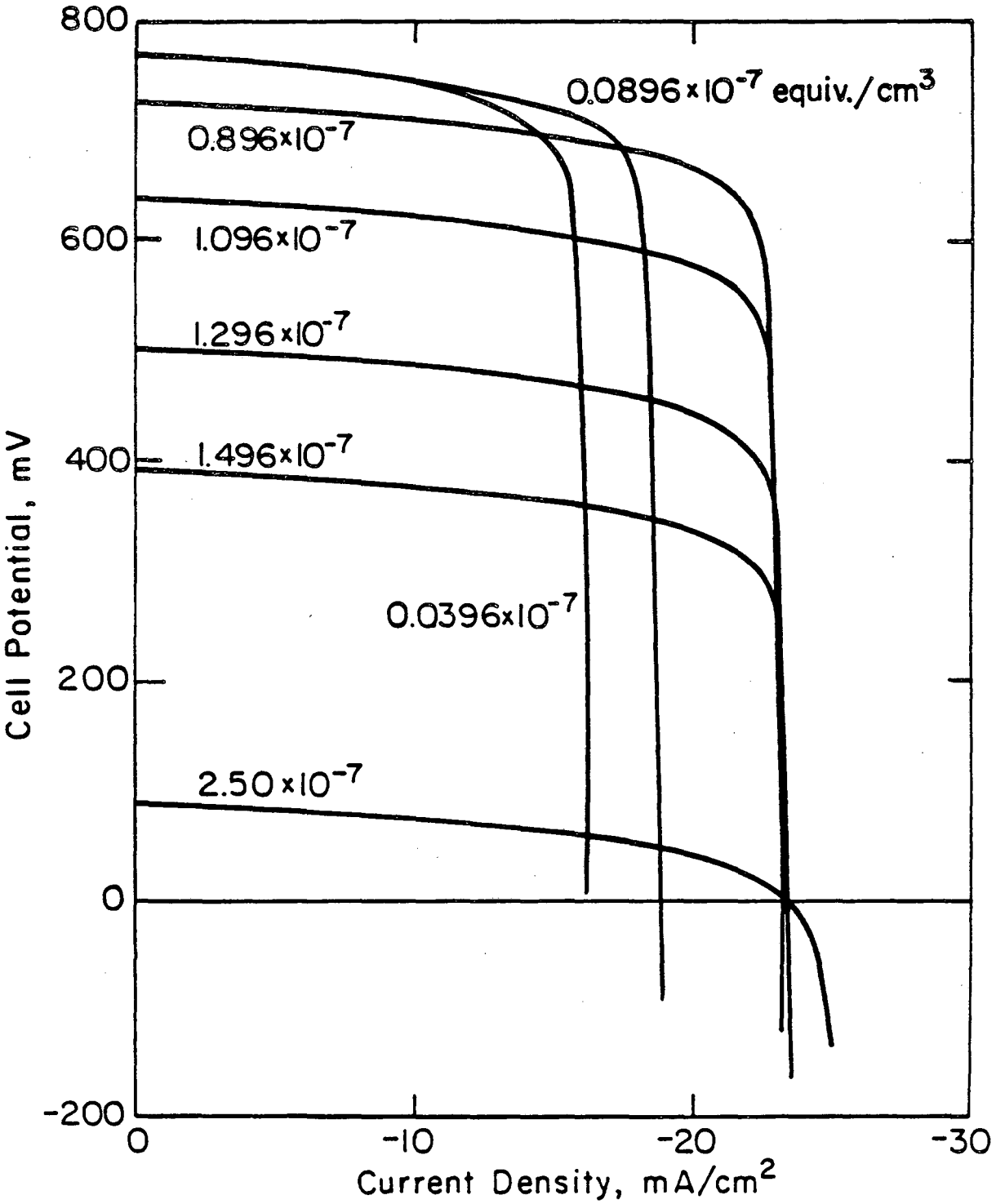

Figure 7. Computed current-potential curves for an n-type GaAs anode with dopant concentration as a parameter.

section 3.2.2). A change in the Debye length influences the utilization of the incident radiation (see section 3.2.3.), but the change in cell performance due to this effect is small.

Maximization of power density yields an optimal dopant concentration for the n-GaAs system of about 9.0×10^{-8} equivalents/cm^3. The donor concentration in the work presented by Heller and Miller[27,28] was 6×10^{16} carriers/cm^3 (or 9.96×10^{-8} equivalents/cm^3).

2.2.2. Semiconductor thickness. The effect of semiconductor thickness on the cell performance is presented in Figure 8 for a characteristic depth of light adsorption of 228.2 A (corresponding to 1.35 Debye lengths). The cell potential increases as the thickness increases from 5 to 13 Debye lengths. The current-potential curve is essentially unchanged for an increase in thickness from 13 to 30 Debye lengths. A very thick semiconductor is expected to decrease the system performance because of resistive losses in the semiconductor. A thin semiconductor limits the cell performance because of saturation of charge in the semiconductor. All mobile electrons are driven from the semiconductor in response to the negatively charged interface, and a large potential gradient across the semiconductor cannot be sustained.

2.2.3. Solar absorption coefficient. The characteristic length for absorption of light can be compared to the Debye length by the dimensionless absorption coefficient $m\lambda_{sc}$. The open circuit cell potential is presented in Figure 9 as a function of the dimensionless absorption coefficient. A maximum in cell potential is observed in the region where the characteristic length for absorption of light is of the same order as the Debye length. The cell potential is relatively insensitive to the dimensionless absorption

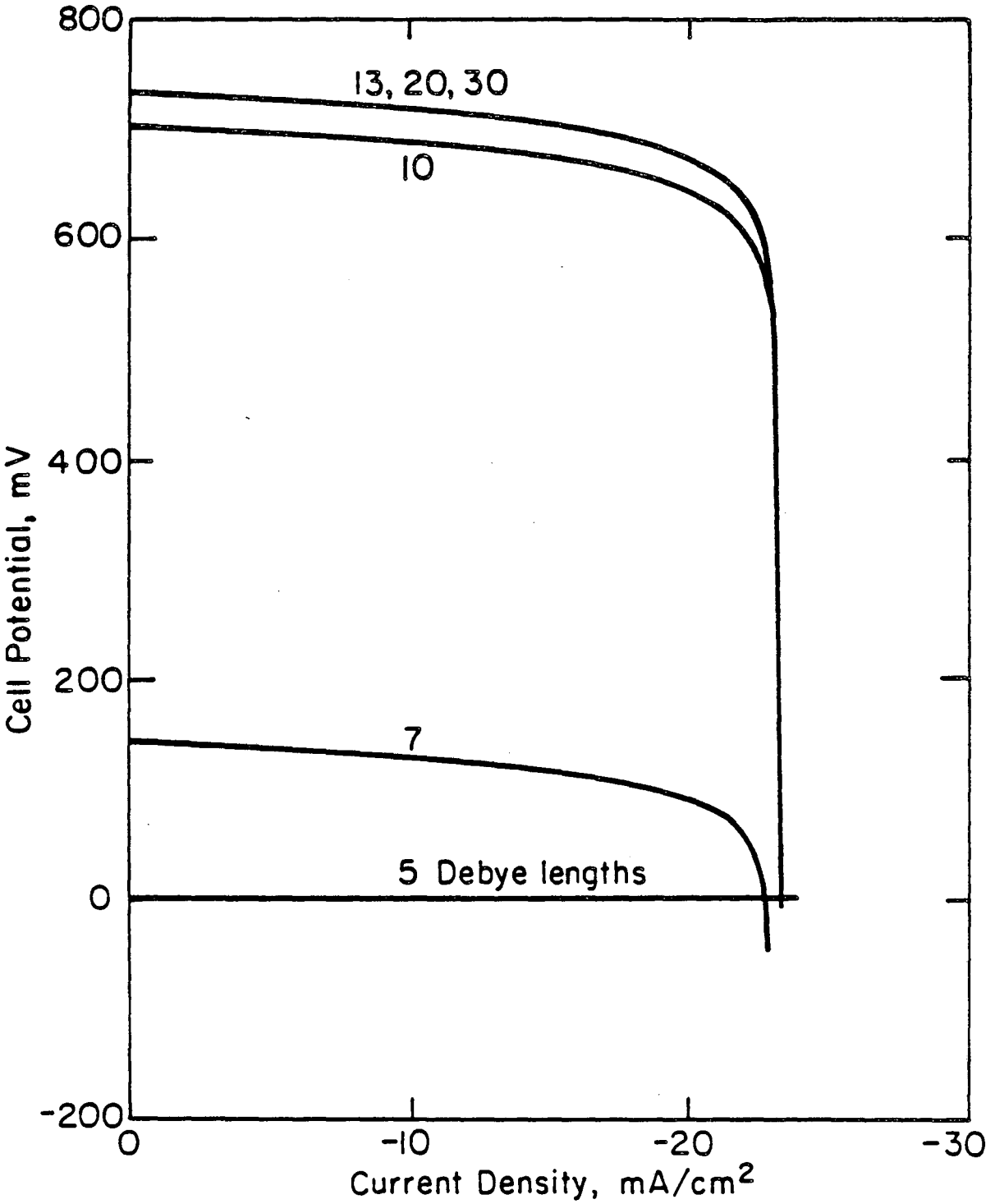

XBL 835-9619

Figure 8. Computed current-potential curves for an n-type GaAs anode with semiconductor thickness as a parameter.

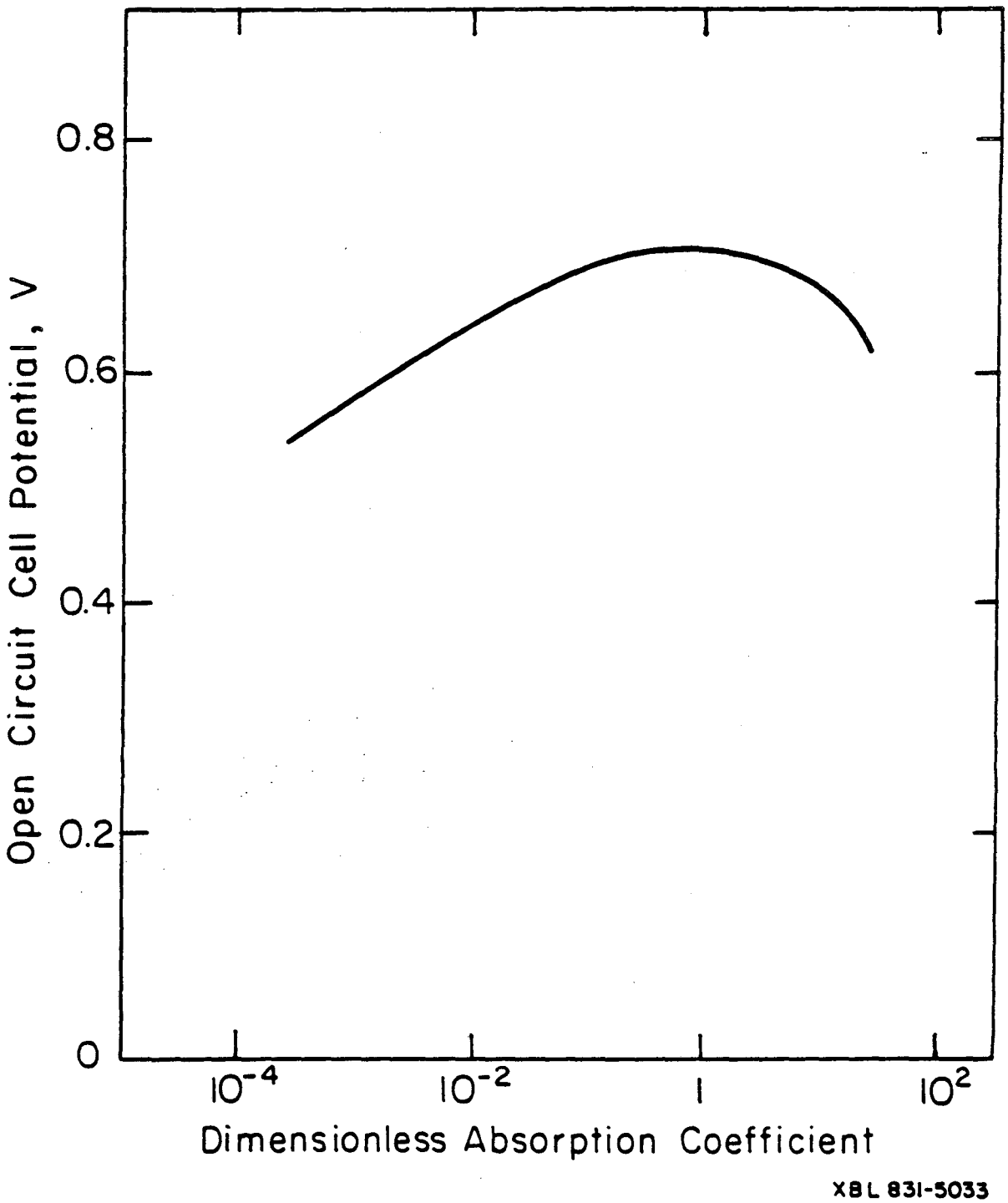

Figure 9. Open-circuit cell potential as a function of dimensionless solar absorption coefficient.

coefficient within the range of 0.2 to 3.0. The optimal value for the dimensionless absorption coefficient was around 0.425, where the characteristic length for light absorption is 2.4 Debye lengths. The absorption coefficient for single crystal GaAs, averaged over photons with energy greater than the band gap energy, is 4.4×10^{-5} cm. This value corresponds to a dimensionless absorption coefficient of 26 and to a characteristic absorption depth of 0.0038 Debye lengths.

2.2.4. Solar flux. The amount of light absorbed within the semiconductor has a strong effect on cell performance. As seen from Figure 10, light scattering or reflective losses can reduce the limiting current from -23.2 mA/cm^2 under full AM-2 irradiation (modeled here with a single mean absorption coefficient) to -14.0 mA/cm^2 under 60 percent of AM-2 irradiation. The 40 percent decrease in limiting current is accompanied by a 1 percent decrease in open-circuit cell potential. The amount of light absorbed within the semiconductor is directly related to the generation of the limiting species, holes, and therefore primarily affects the limiting current.

2.3. Cell Design

Under electrolyte-side illumination and without interfacial kinetic limitations, electrolyte resistance, and counterelectrode effects, the maximum power efficiency of the cell was calculated to be 15.0 percent. This is the value that one might observe if the power density is calculated using a potential drop measured between the semiconductor electrode and a reference electrode reversible to the redox reaction and located just outside the diffusion region. The resistance of the electrolyte, mass-transfer and kinetic limitations at the counterelectrode, and the choice of

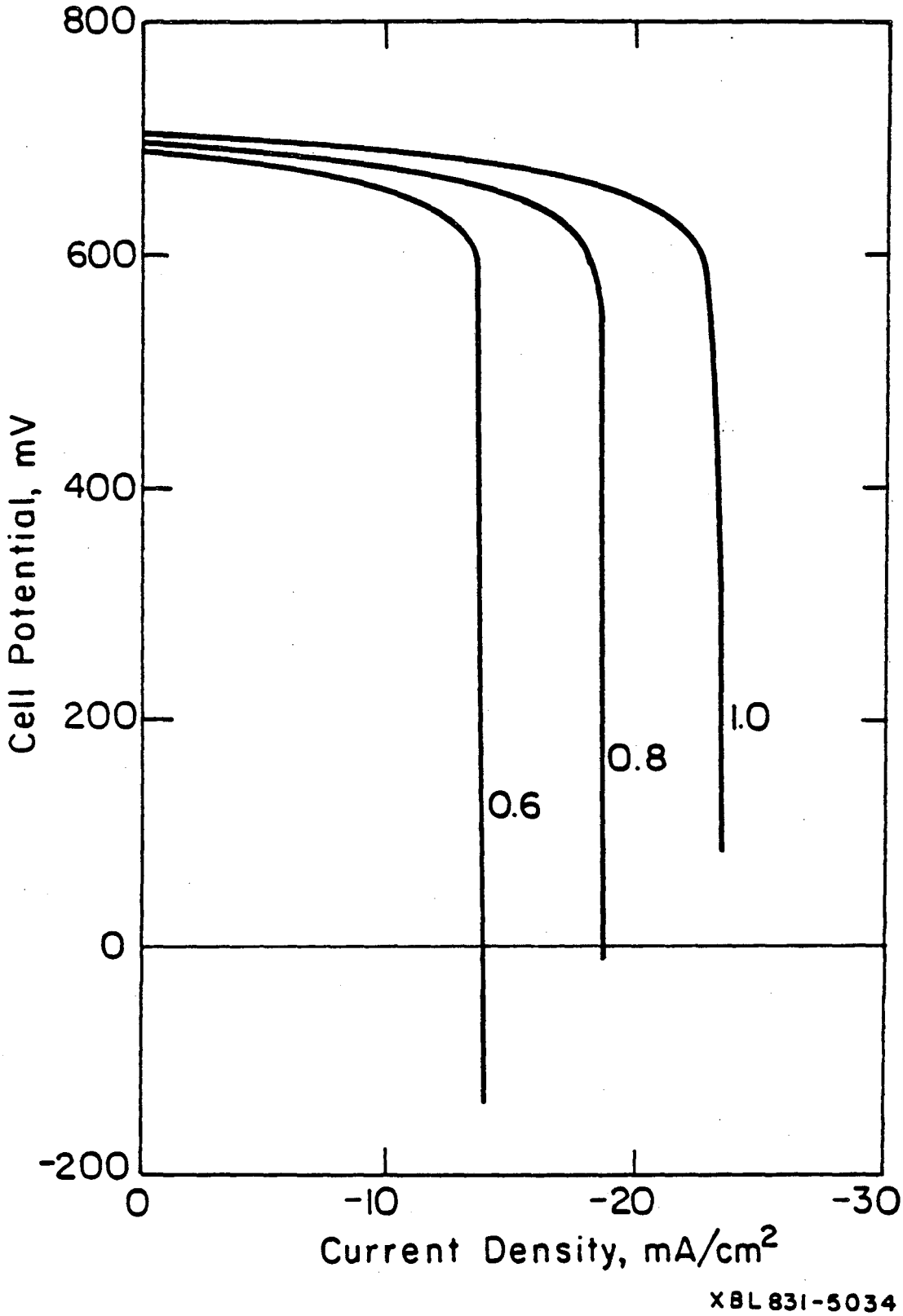

Figure 10. Computed current-potential curves for an n-type GaAs anode with fractional absorption of incident AM-2 radiation as a parameter.

front or back-illumination will affect this value.

2.3.1. Electrolyte and counterelectrode. Resistance in the electrolyte and kinetic and mass-transfer effects at the counterelectrode decrease the maximum power-density of the liquid-junction photovoltaic cell. The current-potential curve for a system with no interfacial kinetic limitations (see Figure 2) is presented in Figure 11 with electrolyte resistance included. The conductivity of the electrolyte was assumed to be 0.3 $\Omega^{-1}cm^{-1}$. The cell potential at a given current is reduced by an amount which is proportional to the current density and to the distance L between the counterelectrode and the semiconductor. A 10 cm separation between the counterelectrode and the semiconductor reduces the maximum power efficiency of the cell to 4 0 percent.

The same base current-potential curve is presented in Figures 12 and 13 with the effect of kinetic and mass transfer limitations at the counterelectrode included. The reaction

$$2Se^{2-} \rightarrow Se_2^{2-} + 2e^- \qquad (2)$$

was assumed to follow the sequence

$$Se^{2-} \rightarrow Se^-_{ads} + e^- . \qquad (3a)$$

$$2Se^-_{ads} \rightarrow Se_2^{2-} . \qquad (3b)$$

Under the assumption that the second step is equilibrated, the current density at the counterelectrode can be expressed by

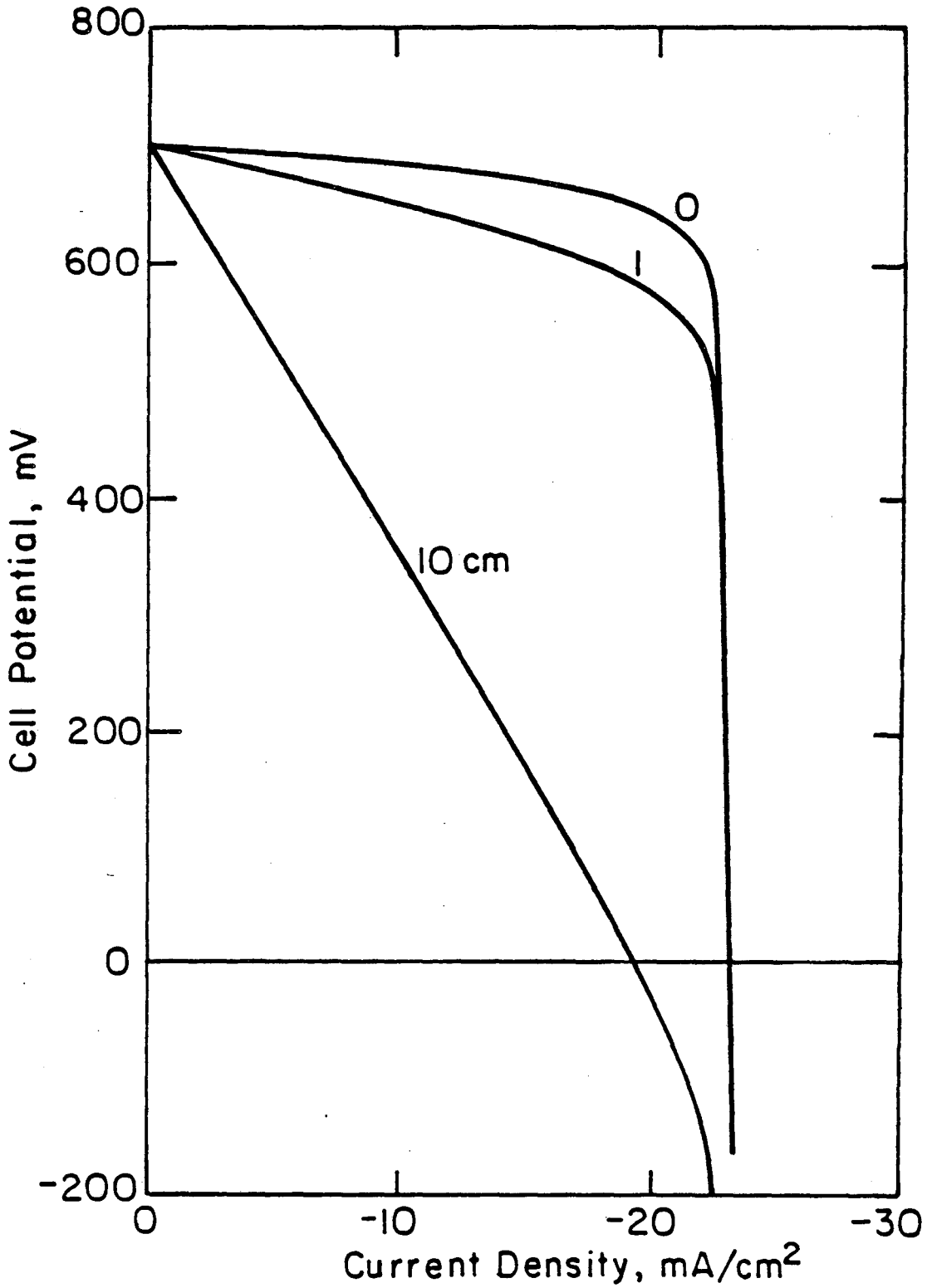

Figure 11. Computed current-potential curves for an n-type GaAs anode with the separation between the counterelectrode and the semiconductor as a parameter. Solution resistance has been included.

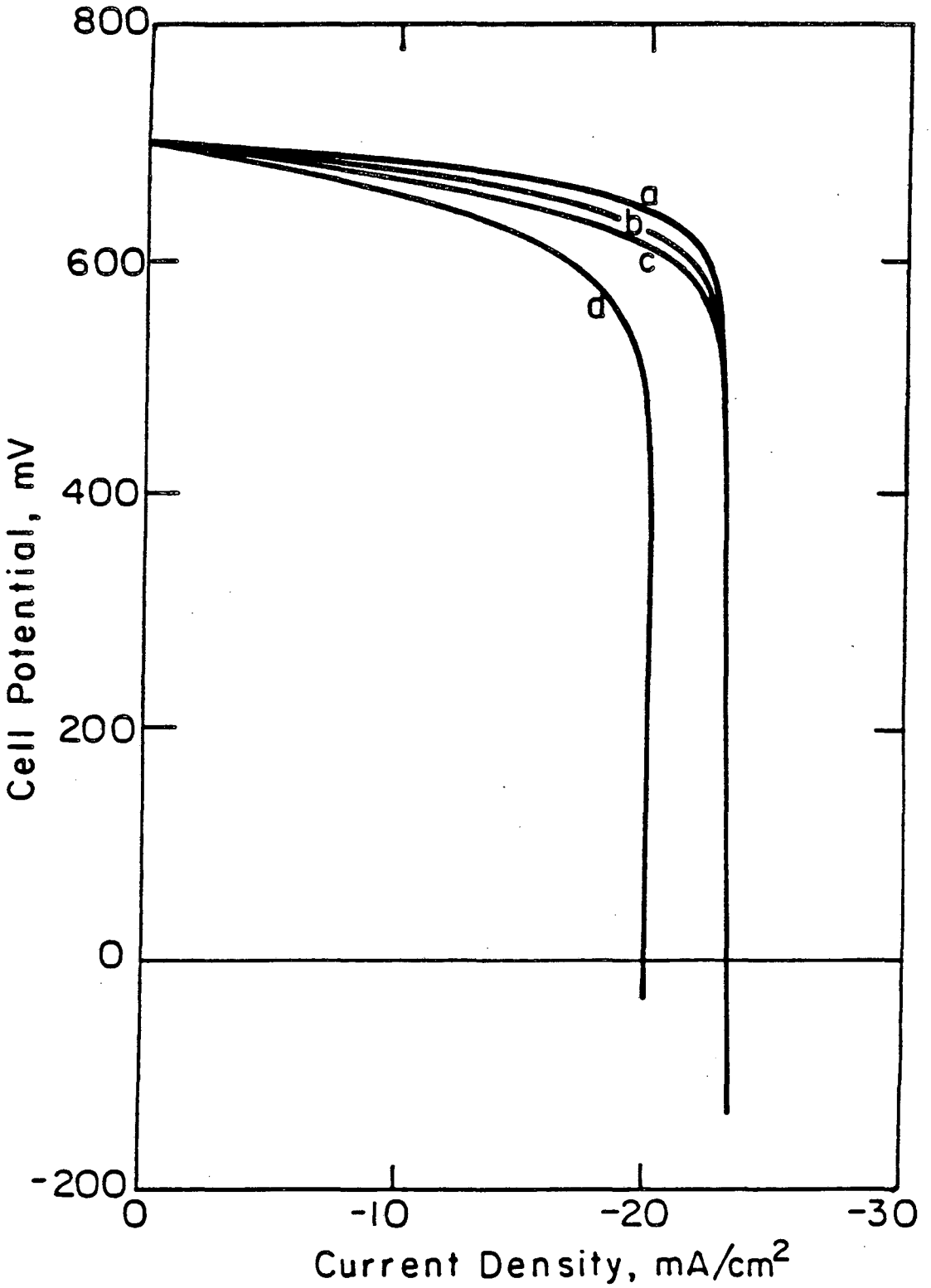

XBL 831-5041

Figure 12. Computed current-potential curves for an n-type GaAs anode with diffusion-limited current density at the counterelectrode as a parameter. Curve a, counterelectrode effects not included; curve b, $i_{lim,3}$= 20 mA/cm^2 and $i_{lim,4}$=80 mA/cm^2; curve c, $i_{lim,3}$=10 mA/cm^2 and $i_{lim,4}$= 40 mA/cm^2; curve d, $i_{lim,3}$=5mA/cm^2 and $i_{lim,4}$=20 mA/cm^2.

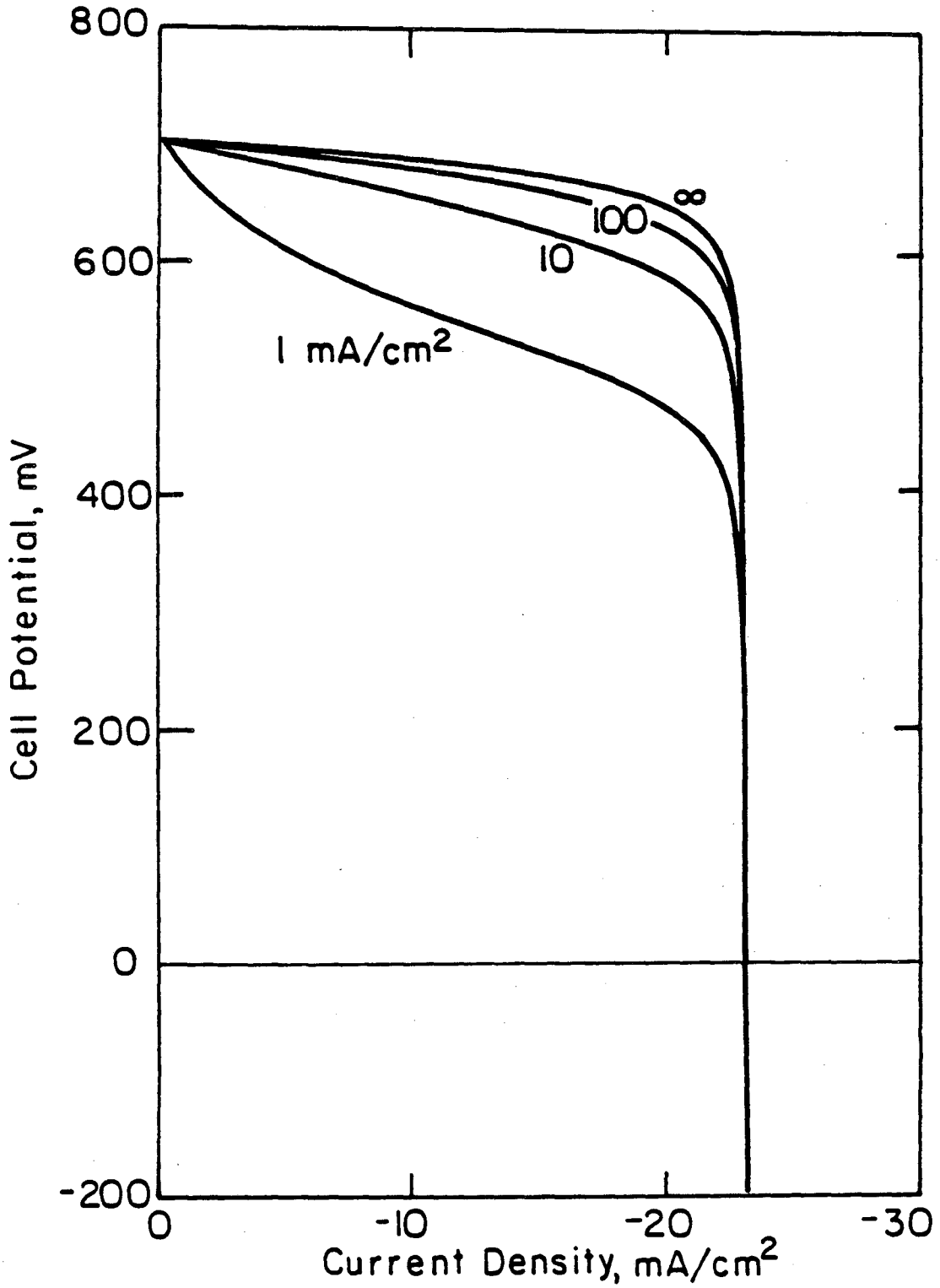

Figure 13. Computed current-potential curves for an n-type GaAs anode with counterelectrode exchange-current density as a parameter. Kinetic and mass-transfer effects at the counterelectrode have been included.

$$i = i_o \left\{ \left[1 - \frac{i}{i_{4,lim}} \right] \exp\left[\frac{(1-\beta)F}{RT} \eta_{CE} \right] - \left[1 + \frac{i}{i_{3,lim}} \right]^{1/2} \exp\left[- \frac{\beta F}{RT} \eta_{CE} \right] \right\}, \quad (4)$$

where i_o is the exchange current density associated with the bulk concentrations of reactants,

$$i_o = F k_{a,f}^{\beta} c_{4,\infty}^{\beta} \left[\frac{k_{a,b} k_{b,b}^{1/2}}{k_{b,f}^{1/2}} c_{3,\infty}^{1/2} \right]^{(1-\beta)},$$

$i_{3,lim}$ is the diffusion-limited current density associated with species Se_2^{2-}, $i_{4,lim}$ is the diffusion-limited current density associated with species Se^{2-}, and n is equal to one.

The effect of diffusion limitation to currents at the counterelectrode is presented in Figure 12 with diffusion-limited current density at the counterelectrode as a parameter. Diffusion-limited current densities of 20 mA/cm^2 for Se_2^{2-} and 80 mA/cm^2 for Se^{2-} correspond to a Nernst stagnant diffusion layer thickness of about 0.010 cm. An exchange-current density of 100 mA/cm^2 was assumed. The influence of the exchange current density on the current-potential curve is presented in Figure 13. Diffusion-limited currents of 20 mA/cm^2 and 80 mA/cm^2 were assumed for the Se_2^{2-} and the Se^{2-} species, respectively. Kinetic limitations, either at the counterelectrode or the semiconductor, cause an inflection point in the current-potential curve.

The calculated maximum power efficiency is 11.8 percent for a cell with a 1.0 cm gap between the semiconductor and the counterelectrode, an exchange current density of 100 mA/cm^2, and diffusion limited currents of 20 mA/cm^2 and 80 mA/cm^2 at the counterelectrode for the Se_2^{2-} and the

Se^{2-} species, respectively. Reduction of illumination due to absorption in the electrolyte and reflection were not included.

2.3.2. Front and back illumination. The semiconductor can be illuminated at the semiconductor-electrolyte interface (front illumination) or at the semiconductor-current collector interface (back illumination). The influence of the direction of illumination is strongly dependent upon the relative rates of recombination in the bulk and at the interfaces involved.

Under the conditions of a negligible surface recombination at the semiconductor-current collector interface and of a small rate of homogeneous recombination as compared to the rate of recombination at the semiconductor-electrolyte interface, back-illumination increases the power output. This effect is illustrated in Figure 14, where current-potential curves for the case with no interfacial kinetic limitations are presented for the semiconductor under front and back-illumination. The limiting current under back-illumination is -25.6 mA/cm^2, and the maximum power efficiency is 17.0 percent. The limiting current under front-illumination is -23.2 mA/cm^2, and the maximum power efficiency is 15.0 percent. Generation of electron-hole pairs in regions where recombination is facilitated reduces the power output.

3. DISCUSSION

Experimental results reported in the literature show the general shape of the current-potential curves presented in this paper. Small scale systems are generally designed with large counterelectrode areas (to minimize any limitation to current flow at the counterelectrode) and a small depth of electrolyte over the semiconductor surface (to minimize losses of

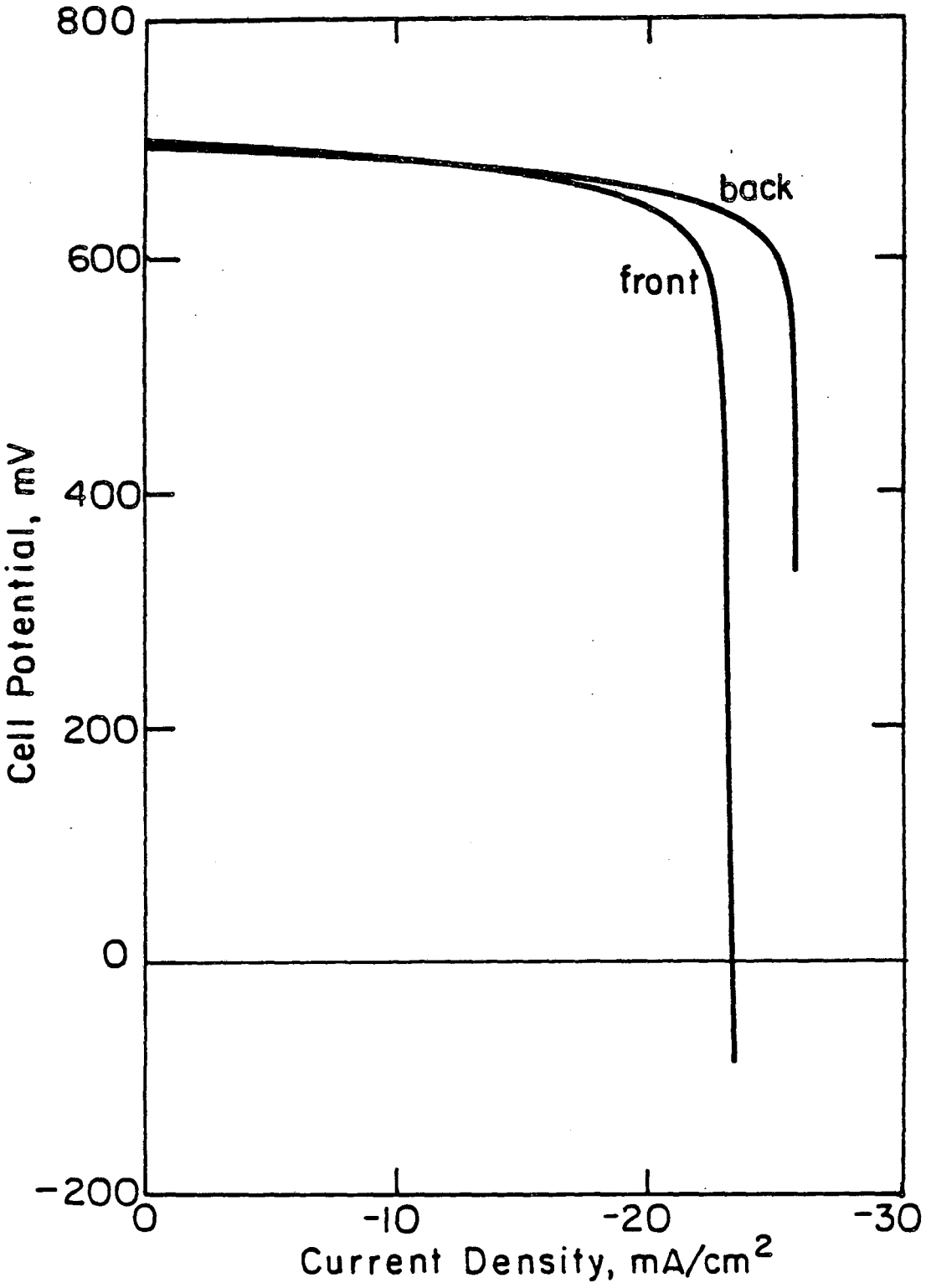

Figure 14. Computed current-potential curves for an n-type GaAs anode with the direction of illumination (front or back illumination) as a parameter.

illumination by absorption in the electrolyte). Current-potential curves thereby obtained include effects of electrolyte resistance and illumination losses.

Inflection points are observed for many experimental systems, e.g., TiO_2 in 1.0 M NaOH,[34] TiO_2 in 0.1 M Na_2SO_4 at pH less than 10 (adjusted with NaOH and H_2SO_4),[35] $PbFe_{12}O_{19}$, $Hg_2Ta_2O_7$, $CdFe_2O_4$, and $Pb_2Ti_{1.5}W_{0.5}O_{6.5}$ in 0.2 M NaOH,[36] n and p-type GaP in liquid ammonia,[37] p-GaP in 0.5 M H_2SO_4,[38] WO_3 in 1 M sodium acetate,[39] $KTaO_3$ in 8.6 M NaOH,[40] CdS in 0.1 M NaOH,[41] CdS in 1.0 M NaI, 1.0 M $Na_2S_2O_3$, and 0.1 M I_2,[42] and untreated polycrystalline GaAs with a selenium redox couple.[8] These inflection points are indicative of kinetic limitations to charge-transfer or to ion-adsorption reactions at the semiconductor-electrolyte interface (as shown by the parameter variation in Figures 2 and 5 in section 3.1). Other systems, e.g., ruthenium-treated polycrystalline GaAs[8,43] and single-crystal GaAs[44] in contact with a selenium redox couple, CdS and Bi_2S_3 in contact with a sulphide-polysulfide redox couple[45], CdS in 1M KCl, 0.8M CH_3COOH, and 0.2 M CH_3COOHa,[46] and p-InP in contact with a vanadium redox couple,[8] do not exhibit inflection points. The interfacial reactions are equilibrated for these systems.

The results of the mathematical model presented in this paper are compared to experimental results in Figure 15. The solid line represents the experimental current-potential curve for a ruthenium-treated n-GaAs photoanode in contact with a selenium redox couple.[27,28] The dashed lines are calculated results in which interfacial reactions were assumed to be equilibrated. Both calculated curves include a seven percent loss of illumination; the lower curve includes an electrolyte resistance of 3 Ω-cm^2. The model parameters are presented in Tables 1, 2, and 3. Bulk transport

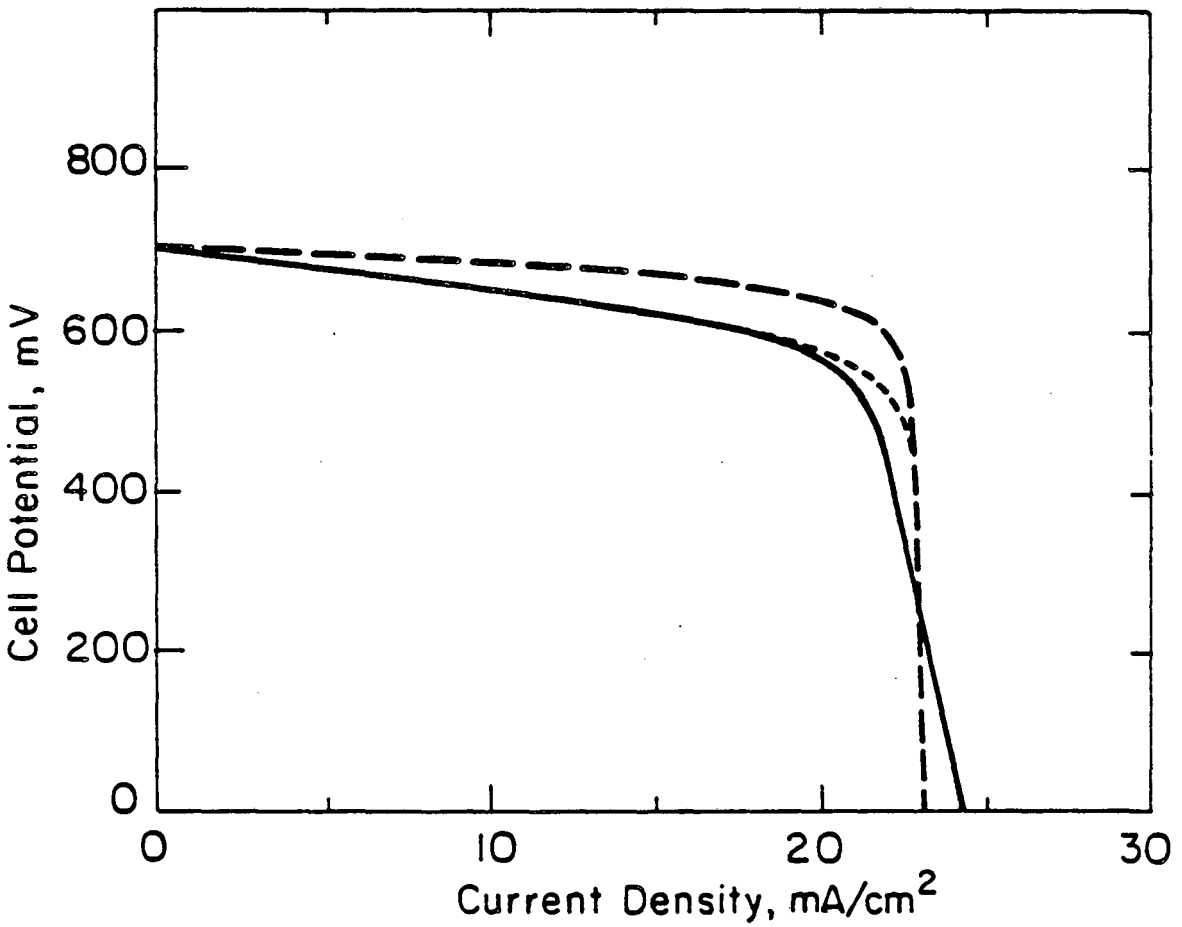

Figure 15. Comparison of computed current-potential curves (dashed lines) to experimental results (solid line) for an n-type GaAs anode in contact with a selenium redox couple.

properties were obtained from the literature; values were assumed for properties characteristic of the semiconductor-electrolyte interface. The model agrees with the experimental results near open circuit but exhibits a sharper limiting-current plateau than the experimental results indicate. An increase in the homogeneous recombination rate constants decreases the sharpness of the potential drop near limiting current but also decreases the cell potential. This change in parameter must be accompanied by an increase in the equilibrium OSS potential (see Chapter 6 of reference (47)). The computer program did not converge at large values of Φ_{oss}.

Some of the model parameters are associated with characteristics of the current-potential curve. In the absence of counterelectrode effects, the magnitude of the limiting current is determined by the intensity of illumination, and the shape of the curve is determined by kinetic parameters. Kinetic limitations to charge-transfer and to ion-adsorption reactions result in an inflection point. Kinetic limitations at the counterelectrode can also cause an inflection point. The magnitude of the open-circuit potential is a function of the equilibrium potential difference between the semiconductor and the solution. Within the model, this parameter is represented by the equilibrium OSS potential. The surface site energy distribution also influences the open-circuit cell potential. These parameters could be varied by selection of different semiconductor-electrolyte combinations. The open-circuit cell potential is also affected by semiconductor properties such as band-gap energy and absorption coefficient.

Analytic models of the liquid-junction cell are described in reference (47). These models can match experimental current-potential curves but

show maxima in electron and hole concentrations near the boundary between space-charge and neutral regions. These maxima were not seen in the results of the mathematical model and are probably due to imposition of boundary or matching conditions between those regions.

4. CONCLUSIONS

Kinetic limitations to interfacial charge-transfer and ion-adsorption reactions drastically reduce the power output of the liquid-junction cell. A small interfacial rate constant is compensated by increased potential and concentration driving forces, thus influencing the cell performance.

The cell performance is strongly influenced by bulk-semiconductor and cell-design properties such as the dopant concentration, the semiconductor thickness, and the amount of light adsorbed in the semiconductor. An optimal dopant concentration and semiconductor thickness can be calculated for a given semiconductor system. The resistance of the electrolyte and kinetic and mass-transfer limitations at the counterelectrode influence cell performance and may play an important role in the optimal design of a liquid-junction photovoltaic cell.

5. ACKNOWLEDGEMENT

This work was supported by the United States Department of Energy under Contract No. DE-AC03-76SF00098 through the Director, Office of Energy Research, Office of Basic Energy Sciences, Chemical Sciences Division, and through the Assistant Secretary of Conservation and Renewable Energy, Office of Advanced Conservation Technology, Electrochemical Systems Research Division.

6. NOTATION

6.1. Roman Characters

c_i	molar concentration of species i, mol/cm^3
D_i	diffusivity of species i, cm^2/s
E_i	energy of species or site i, eV
ΔE_i	ionic adsorption energy, J/mol
f_i	molar activity coefficient of species i
F	Faraday's constant, 96,487 C/equiv
G_{th}	rate of thermal electron-hole pair generation, mol/s-cm^3
G_L	rate of photo electron-hole pair generation, mol/s-cm^3
i	current density, mA/cm^2
i_o	exchange current density, mA/cm^2
$k_{f,l}$	forward reaction rate constant for reaction l
$k_{b,l}$	backward reaction rate constant for reaction l
k_k	rate constants for homogeneous reaction k
K_l	equilibrium constant for reaction l
m	solar absorption coefficient, 1/cm
M_i	symbol for chemical formula of species i
n	number of electrons involved in electrode reaction
n	electron concentration, mol/cm^3
n_i	intrinsic electron concentration, mol/cm^3
N	total site concentration, mol/cm^3
N_a	total bulk electron-acceptor concentration, mol/cm^3

N_d	total bulk electron-donor concentration, mol/cm^3
N_i	flux of species i, mol/cm^{2}s
p	hole concentration, mol/cm^3
$p_{i,l}$	heterogeneous reaction order
$q_{i,l}$	heterogeneous reaction order
q_o	incident solar flux, mol/s-cm^2
r_l	heterogeneous reaction rate, mol/s-cm^2
R	universal gas constant, 8.3143 J/mol-K
R_i	net rate of production of species i, mol/s-cm^3
R_{rec}	net rate of electron-hole recombination, mol/s-cm^3
s_i	stoichiometric coefficient of species i in an electrode reaction
T	absolute temperature, K
u_i	mobility of species i, cm^2-mol/J-s
V	potential drop across depletion layer, V
W	depletion layer thickness, cm
y	distance variable, cm
z_i	charge number of species i

6.2. Greek Characters

β	symmetry factor
γ_k	surface concentration of energy or species k, mol/cm^2
Γ_k	total surface-site concentration of energy or species k, mol/cm^2

δ_k	distance between interfacial planes (gap denoted by k), cm
ε	permittivity, C/V-cm
η	photon efficiency
η_k	total overpotential at interface k, V
Θ	fractional occupation of surface sites
κ	conductivity, mho/cm
λ	Debye length, cm
μ_i	electrochemical potential of species i, J/mol
Φ	electrical potential, V

6.3. Superscripts

o	equilibrium
ϑ	secondary reference state at infinite dilution
$*$	secondary reference state in semiconductor

6.4. Subscripts

bulk	associated with the bulk
c	associated with conduction band in semiconductor
CE	associated with the counterelectrode
cell	associated with the cell
e^-	relating to electrons
h^+	relating to holes
ihp	associated with inner Helmholtz plane
iss	associated with inner surface states
k	dummy subscript
l	associated with reaction *l*

o	equilibrium value or initial value
ohp	associated with outer Helmholtz plane
oss	associated with outer surface states
sc	associated with semiconductor
sol	associated with solution
t	associated with trap band in semiconductor
v	associated with valence band in semiconductor
1	associated with the region between the OSS and the ISS
2	associated with the region between the ISS and the IHP
3	associated with the region between the IHP and the OHP

7. REFERENCES

[1] Fujishima, Akira, and Kenichi Honda, "Electrochemical Photolysis of Water at a Semiconductor Electrode," *Nature*, *238* (1972), 37-38.

[2] Manassen, J., D. Cahen, and G. Hodes, "Electrochemical, Solid State, Photochemical, and Technological Aspects of Photoelectrochemical Energy Converters," *Nature*, *263* (1976), 97-100.

[3] Bard, Allen J., "Photoelectrochemistry and Heterogeneous Photocatalysis at Semiconductors," *Journal of Photochemistry*, *10* (1979), 59-75.

[4] Ehrenreich, H. and J. H. Martin, "Solar Photovoltaic Energy," *Physics Today*, *32*, 9 (1979), 25-32.

[5] Wrighton, Mark S., "Photoelectrochemical Conversion of Optical Energy to Electricity and Fuels," *Accounts of Chemical Research*, *12* (1979), 303-310.

[6] Gerischer, Heinz, "Heterogeneous Electrochemical Systems for Solar Energy Conversion," *Pure and Applied Chemistry*, *52* (1980), 2649-2667.

[7] Bard, Allen J., "Photoelectrochemistry," *Science*, *207* (1980), 139-144.

[8] Heller, Adam, "Conversion of Sunlight into Electrical Power and Photoassisted Electrolysis of Water in Photoelectrochemical Cells," *Accounts of Chemical Research*, *14* (1981), 154-162.

[9] Green, Mino, "Electrochemistry of the Semiconductor-Electrolyte Interface," *Modern Aspects of Electrochemistry*, Volume 2, J. O'M Bockris, editor, Academic Press Inc., New York, 1959.

[10] Gerischer, Heinz, "Semiconductor Electrode Reactions," Chapter 4 in *Advances in Electrochemistry and Electrochemical Engineering*, Volume 1, Paul Delahay, editor, Interscience Publishers, New York, 1961.

[11] Archer, M.D., "Electrochemical Aspects of Solar Energy Conversion," *Journal of Applied Electrochemistry*, *5* (1975), 17-38.

[12] Rajeshwar, K., P. Singh, and J. DuBow, "Energy Conversion in Photoelectrochemical Systems: A review," *Electrochimica Acta*, *23* (1975), 1117-1144.

[13] Harris, L. A., and R. H. Wilson, "Semiconductors for Photoelectrolysis," *Annual Reviews in Materials Science*, *8* (1978), 99-134.

[14] Nozik, Arthur, J., "Photoelectrochemistry: Applications to Solar Energy Conversion," *Annual Reviews in Physical Chemistry*, *29* (1978), 189-222.

[15] Tomkiewicz, M., and H. Fay, "Photoelectrolysis of Water with Semiconductors," *Applied Physics*, *18* (1979), 1-28.

[16] Wilson, R.H., "Electron Transfer Processes at the Semiconductor-Electrolyte Interface," *CRC Critical Reviews in Solid State and Materials Science*, (1980), 1-41.

[17] Memming, R., "Solar Energy Conversion by Photoelectrochemical Processes," *Electrochimica Acta*, *25* (1980), 77-88.

[18] Morrison, S. Roy, *Electrochemistry at Semiconductor and Oxidized Metal Electrodes*, Plenum Press, New York, 1980.

[19] Khan, Shahed U. M., and John O'M. Bockris, "Photoelectrochemical Kinetics and Related Devices," Chapter 3 in *Modern Aspects of Electrochemistry*, Volume 14, J. O'M. Bockris, B. E. Conway, and R. E. White, editors, Plenum Press, New York, 1982.

[20] Orazem, Mark E. and John Newman, "Mathematical Modeling of Liquid-Junction Photovoltaic Cells: I. Governing Equations," submitted to *the Journal of the Electrochemical Society*, (LBL-16210).

[21] Orazem, Mark E. and John Newman, "Mathematical Modeling of Liquid-Junction Photovoltaic Cells: III. Optimization of Cell Configurations," submitted to *the Journal of the Electrochemical Society*, (LBL-16212).

[22] Grahame, David C., "The Electrical Double Layer and the Theory of Electrocapillarity," *Chemical Reviews*, *41* (1947), 441-501.

[23] Dewald, J. F., "Semiconductor Electrodes," Chapter 17 in *Semiconductors*, N. B. Hannay, editor, Reinhold Publishing Corporation, New York, 1959.

[24] Sparnaay, Marcus Johannes, *The Electrical Double Layer*, Pergamon Press, New York, 1972.

[25] Orazem, Mark E., and John Newman, "Theoretical Analysis of Liquid-Junction Photovoltaic Cells," 159th meeting of *the Electrochemical Society*, Minneapolis, Minnesota, May 14, 1981.

[26] Newman, John, "Numerical Solution of Coupled, Ordinary Differential Equations," *Industrial and Engineering Chemistry Fundamentals*, *7* (1968), 514-517.

[27] Heller, Adam, and B. Miller, "Photoelectrochemical Solar Cells: Chemistry of the Semiconductor-Liquid Junction," Chapter 12 in *Interfacial Photoprocesses: Energy Conversion and Synthesis, Advances in Chemistry Series, 184*, Mark S. Wrighton, editor, American Chemical Society, Washington D. C., 1980.

[28] Parkinson, B. A., A. Heller, and B. Miller, "Enhanced Photoelectrochemical Solar-Energy Conversion by Gallium-Arsenide Surface Modification," *Applied Physics Letters*, *33* (1978), 521-523.

[29] Heller, A., K. C. Chang, and B. Miller, "Spectral Response and Efficiency Relations in Semiconductor Liquid Junction Solar Cells," *Journal of the Electrochemical Society*, *124* (1977), 697-700.

[30] Chang, K. C., A. Heller, B. Schwartz, S. Menezes, and B. Miller, "Stable Semiconductor Liquid-Junction Cell with 9% Solar to Electrical Conversion Efficiency," *Science*, *196* (1977), 1097-1098.

[31] Ellis, Arthur B., Jeffrey M. Bolts, Steven W. Kaiser, and Mark S. Wrighton, "Study of n-Type Gallium Arsenide- and Gallium Phosphide-Based Photoelectrochemical Cells. Stabilization by Kinetic Control and Conversion of Optical Energy to Electricity," *Journal of the American Chemical Society*, *99* (1977), 2848-2854.

[32] Wrighton, Mark S., Jeffrey M. Bolts, Andrew B. Bocarsly, Michael C. Palazzotto, and Erick G. Walton, "Stabilization of n-Type Semiconductors to Photoanodic Dissolution: II-VI and III-V Compound Semiconductors and Recent Results for n-Type Silicon," *Journal of Vacuum Science Technology*, *15* (1978), 1429-1435.

[34] Nakato, Yoshihiro, Nobuyuki Takamori, and Hiroshi Tsubomura, "A Composite Semiconductor Photoanode for Water Electrolysis," *Nature*, *295* (1982), 312-313.

[35] Gissler, W., P. L. Lensi, and S. Pizzini, "Electrochemical Investigation of an Illuminated TiO_2 Electrode," *Journal of Applied Electrochemistry*, *6*

(1976), 9-13.

[36] Kung, H. H., H. S. Jarrett, A. W. Sleight, and A. Ferretti, "Semiconducting Oxide Anodes in Photoassisted Electrolysis of Water," *Journal of Applied Physics*, *48* (1977), 2463-2469.

[37] Belloni, Jacqueline, Genevieve Van Amerongen, Michel Herlem, Jean-Lou Sculfort, and Rudolf Heindl, "Photocurrents from Semiconductor-Liquid Ammonia Junctions," *Journal of Physical Chemistry*, *84* (1980), 1269-1270.

[38] Dare-Edwards, M. P., A. Hamnett, and J. B. Goodenough, "The Efficiency of Photogeneration of Hydrogen at P-Type III/V Semiconductors," *Journal of Electroanalytical Chemistry*, *119* (1981) 109-123.

[39] Butler, M. A., R. D. Nasby, and Rod K. Quinn, "Tungsten Trioxide as an electrode for Photoelectrolysis of Water," *Solid State Communications*, *19* (1976), 1011-1014.

[40] Ellis, Arthur B., Steven W. Kaiser, and Mark S. Wrighton, "Semiconducting Potassium Tantalate Electrodes. Photoassistance Agents for the Efficient Electrolysis of Water," *Journal of Physical Chemistry*, *80* (1976), 1325-1328.

[41] Memming, R., "A Rotating Platinum-Semiconductor Ring-Disc Electrode for Analysis of Photoelectrochemical Processes," *Berichte der Bunsengesellschaft fur Physikalische Chemie*, *81* (1977), 732-735.

[42] Gerischer, H. and J. Gobrecht, "On the Power-Characteristics of Electrochemical Solar Cells," *Berichte der Bunsengesellschaft fur Physikalische Chemie*, *80* (1976), 327-330.

[43] Johnston, Jr., W. D., H. J. Leamy, B. A. Parkinson, A. Heller, and B. Miller, "Effect of Ruthenium Ions on Grain Boundaries in Gallium Arsenide Thin Film Photovoltaic Devices," *Journal of the Electrochemical Society*, *127* (1980), 90-95.

[44] Gerischer, H., "On the Stability of Semiconductor Electrodes Against Photodecomposition," *Journal of Electroanalytical Chemistry*, *82* (1977), 133-143.

[45] Miller, Barry, and Adam Heller, "Semiconductor Liquid Junction Solar Cells Based on Anodic Sulphide Films," *Nature*, *262* (1976), 680-681.

[46] Vanden Berghe, R. A. L., W. P. Gomes, and F. Cardon, "Some Aspects of the Anodic Behavior of CdS Single Crystals in Indifferent Electrolyte Solutions," *Berichte der Bunsengesellschaft fur Physikalische Chemie*, *77* (1973), 289-293.

[47] Orazem, Mark E., *Mathematical Modeling and Optimization of Liquid-Junction Photovoltaic Cells*, Ph.D. thesis, University of California, Berkeley, June, 1983 (LBL-16131).

TECHNICAL INFORMATION DEPARTMENT
LAWRENCE BERKELEY LABORATORY
UNIVERSITY OF CALIFORNIA
BERKELEY, CALIFORNIA 94720